Materials Advances

ROYAL SOCIETY OF CHEMISTRY

PAPER

View Article Online
View Journal | View Issue

Check for updates

Cite this: *Mater. Adv.*, 2023, 4, 2119

High birefringence liquid crystals with a wide temperature range and low melting point for augmented reality displays†

Ran Chen,[a] Liang Zhao,[a] Yannanqi Li,[b] Jian Li,[c] Pei Chen,[a] Xinbing Chen *[a] and Zhongwei An *[ac]

Received 25th January 2023,
Accepted 30th March 2023

DOI: 10.1039/d3ma00042g

rsc.li/materials-advances

A series of tolane liquid crystals terminated by but-3-enyl with high performance (such as high clearing point, low melting point, high birefringence Δn, low viscosity γ_1, and broad nematic phase interval) were designed and synthesized in accordance with the phase-only liquid-crystal-on-silicon (LCoS) device requirements for AR displays. The effects of the lateral fluoro-substituent, central alkyne bond, terminal group, and flexible *n*-alkyl chain on the thermal properties were systematically investigated, and density functional theory (DFT) calculations of molecular conformation and aspect ratio were used to corroborate the experimental results. Further, their properties of phase transition temperature, birefringence, and viscosity were comprehensively evaluated in two typical LC mixtures (**001**, **P02-F**). The results indicate that our target compounds can effectively lower the melting point, broaden the working temperature interval, and maintain a high Δn and low γ_1 for three LC mixtures. One new LC mixture by employing compound **2TFV** as a LC dopant exhibited a high Δn (~0.26), moderate γ_1 and dielectric anisotropy (~6.3), and broad temperature adaptability (−31.3 °C to 91.3 °C), and achieved 2.08π phase modulation, 5 V operation voltage, and 2.89 ms response time at 40 °C in a reflective LCoS device.

1. Introduction

Broad temperature adaptability is a key performance evaluator for the widespread applications of all optoelectronic devices, which have attracted significant attention in various fields, such as proton exchange membrane fuel cells,[1,2] perovskite solar cells,[3,4] lithium ion batteries,[5–7] supercapacitors,[8,9] and liquid crystal (LC) devices.[10–13] Augmented reality (AR) displays, one of the emerging research hotspots of LC devices,[14–17] are subject to device failure at low temperature resulting from the temperature-dependent properties of the LC materials used in AR displays. Therefore, there is an urgent need to find effective ways to lower the working temperature of LC devices to enhance their ambient temperature tolerance.

Currently, there are three common methods to improve the low-temperature performance of LC devices: high driving voltage,[18] external auxiliary heating,[19,20] and low-temperature reinforcement technology.[21] Although their ambient temperature tolerance can be improved with the help of the outside world, the low-temperature performance of LC devices depends mainly on the LC mixtures used. Therefore, the most direct and effective way is to develop LC mixtures with a low melting point (T_m) and wide working temperature range. As we know, the LC materials used in AR displays require high birefringence (Δn) to obtain 2π phase modulation and a fast response time.[22–25] Unfortunately, the high Δn property requires large π–π conjugations in LC molecules,[26–28] which inevitably lead to increased intermolecular interaction, further increasing the T_m of LC mixtures and making them unusable. In order to develop practical LC mixtures for AR displays, we usually start with fine molecular engineering strategies to arrange the synthons for LC compounds with excellent performance and then blend them to form one LC mixture with the desired properties.[29] LC mixtures are mainly formulated by mixing an optical regulatory component, an electrical regulatory component, a LC diluter, and a wide-temperature modulation component.[30] The preferred optical regulatory components adopt a tolane or bistolane unit as the molecular skeleton to obtain high Δn and low T_m.[31–33] Lateral fluorine substituents and terminal polar groups

[a] *Key Laboratory of Applied Surface and Colloid Chemistry (MOE), International Joint Research Center of Shaanxi Province for Photoelectric Materials Science, Shaanxi Key Laboratory for Advanced Energy Devices, Shaanxi Engineering Laboratory for Advanced Energy Technology, School of Materials Science and Engineering, Shaanxi Normal University, Xi'an 710062, China. E-mail: chenxinbing@snnu.edu.cn, gmecazw@163.com*
[b] *College of Optics and Photonics, University of Central Florida, Orlando, FL, USA*
[c] *Xi'an Modern Chemistry Research Institute, Xi'an 710065, China*

† Electronic supplementary information (ESI) available. See DOI: https://doi.org/10.1039/d3ma00042g

are utilized to obtain electrical regulatory components with large dielectric anisotropy ($\Delta\varepsilon$) and low T_m.[34,35] LC diluters containing an olefin terminal group have been reported to display low T_m and rotational viscosity (γ_1).[36] Wide-temperature modulation components with a high clearing point (T_c) and relatively low T_m are realized with three-ring molecular structures.[37–39] Overall, these individual parameters (such as high Δn, large $\Delta\varepsilon$, low γ_1, high T_c, and low T_m) or combined parameters have been achieved in one component through molecular engineering strategies. However, there is still a lack of theoretical guidance to realize the required properties of high Δn, large $\Delta\varepsilon$, low γ_1, high T_c and low T_m in one LC mixture for AR displays.

From the aforementioned information, we proposed to design and synthesize target compounds with high performance (broadened nematic phase interval, low T_m, high Δn, high T_c and relatively low γ_1) and further employ them to improve the ambient temperature tolerance of a high-Δn LC mixture for AR displays. As shown in Fig. 1, our molecular tailoring strategy is summarized as follows: (1) one tolane central core was adopted as the molecular skeleton to achieve high Δn, low T_m and low γ_1; (2) many functional groups, including a *trans*-cyclohexyl core,[40,41] ethylene bridge,[41,42] buty-3-enyl terminal group[43] and lateral fluorine atom,[44–46] were introduced to decrease the melting point; (3) the three-ring molecular structure was utilized to maintain high T_c and the broaden LC phase interval.[47] Meanwhile, the effects of the lateral fluoro-substituent, central alkyne bond, terminal group and flexible *n*-alkyl chain on the thermal properties were systematically investigated. Research results indicate that the target compounds meet our molecular design goal; thus, they were further employed as LC dopants in one LC mixture to achieve 2π phase modulation at 5 V driving voltage and a 240 Hz frame rate for AR displays.

2. Experimental section

2.1. Materials

Tetrabutylammonium bromide (TBAB) and tetrakis(triphenylphosphine) palladium ($Pd(PPh_3)_4$) were purchased from Aladdin Reagent Company. Trimethylamine (Et_3N), tetrahydrofuran (THF), potassium hydroxide (KOH), methylbenzene (PhMe) and other reagents were purchased from Sinophinese Chemical Reagent Company. The 2-(4-bromophenethyl)-1,3-dioxolane, 2-(4-bromo-3-fluorophenethyl)-1,3-dioxolane and methyltriphenylphosphonium bromide (CH_3BrPPh_3) were purchased from Xi'an Caijing Opto-Electrical Science & Technology Co. Ltd and used as received. The parent LC mixture (**001**, Δn = 0.0790, T_m = 9.4 °C, T_c = 112.9 °C, γ_1 = 141.4 mPa s) was provided by Xi'an Modern Chemistry Research Institute. The synthesis procedures and characterized data of target compounds are shown in the ESI.†

2.2. Characterization and measurements

Four traditional spectral methods were used, including ^{1}H-nuclear and ^{13}C-nuclear magnetic resonance (^{1}H NMR and ^{13}C NMR) spectra (ECZ400R/S1, Nippon Electronics Co), Fourier transform infrared spectrometry (IR, FTIR Tensor27, Brucker, Germany) and gas phase mass spectrometry (GC-MS, DSQ II, Thermo Fisher Scientific Co., LTD). High performance liquid chromatography (HPLC, LC-20AT, Shimadzu International Trading Co., LTD) and gas chromatography (GC, GC-2014C, Shimadzu, Japan) were employed to detect the purities of the target compounds and intermediates.

Gaussian 09 software was employed to carry out DFT calculations for our target compounds by applying the B3LYP/6-311G (d,p) method[48,49] and we obtained their molecular steric configurations and molecular aspect ratios. Their geometric data are listed in the electronic supplementary information. In addition, frequency calculations were performed to ascertain whether the optimized geometry is without any imaginary frequency. The mesomorphic properties of target compounds **4TV**, ***n*TFV**, **4FTV** and **4FTFV** were tested by differential scanning calorimeter (DSC) and polarizing optical microscope (POM). Under an N_2 atmosphere, the Shimadzu DSC-60 instrument was utilized to measure the phase transition temperatures with a heating/cooling rate of 10 °C min^{-1}. The POM (LEICA DM2500P) instrument was equipped with a Linkam

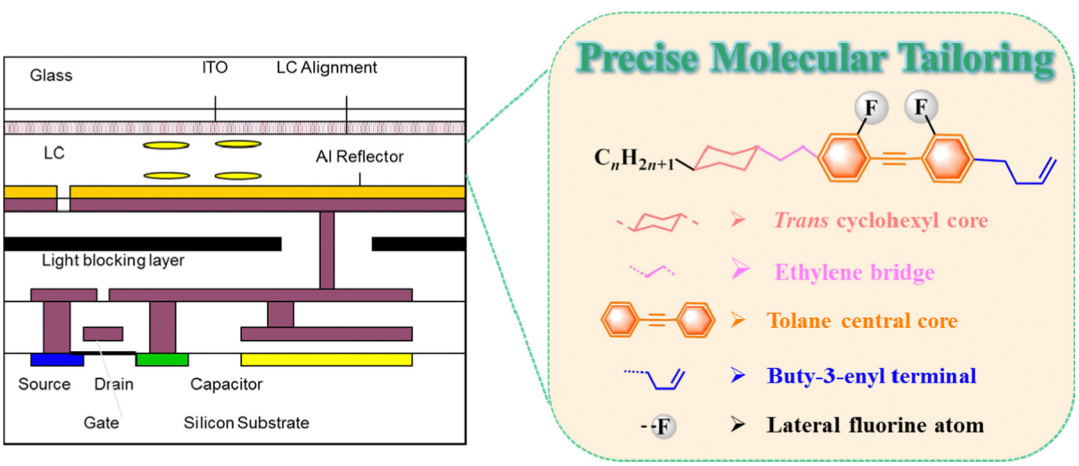

Fig. 1 Molecular tailoring strategy of target compounds with many cooperating functional groups for LCoS devices in AR displays.

THMS600 hot stage to observe the liquid crystal phase state. The phase transition temperatures of LC mixtures were measured by DSC (TA Instruments Q100) in nitrogen at heating/cooling rate of 2 °C min^{-1}.

The molecular structures and compositions of the fluorotolane-based LC mixture **P02-F** have been previously reported.[36] The target compounds **4TV**, **4TFV**, **4FTV**, **4FTFV** and **2TFV** were added into parent LC mixture **001** at a mass fraction of 15% to prepare five new LC mixtures, termed **A**, **B**, **C**, **D** and **E**, respectively. Their Δn values were measured at 20 °C by an Abbe refractometer using a 589 nm wavelength light source, then extrapolated experimental results were obtained by the host–guest method. Their γ_1 values were measured at 25 °C by a multi-channel liquid crystal evaluation system (Model 6254, TOYO Corporation, Japan). Compound **2TFV** (15 wt%) was dissolved in the LC mixture **P02-F** to prepare a new LC mixture **F**. The Δn and γ_1 values of the LC mixtures (**P02-F**, **F**, **SNUP03** and **SNUP04**) were calculated by the measured phase retardation and transient current methods.[50] The dielectric anisotropy ($\Delta\varepsilon$) values of LC mixtures **SNUP03** and **SNUP04** were measured with a multifrequency LCR meter (HP-4274). All measurements for LC mixtures (**P02-F**, **F**, **SNUP03** and **SNUP04**) were carried out at a temperature of 40 °C and a wavelength of 633 nm.

3. Results and discussion

3.1. Synthesis and characterization

All the chemicals were from commercial suppliers and used without further purification. The aryl iodine compounds **nxI** were synthesized through sequential Grignard reaction, Wolff–Kishner-Huang-Minlon reduction reaction and iodization, in accordance with our previous work.[51] Many efficient methods have been reported to create tolane LCs, mainly including the elimination reaction of alkenyl halide, the Sonogashira coupling reaction and the Fritsch–Buttenberg–Wiechell rearrangement. Currently, the most efficient method seems to be the Sonogashira reaction; therefore, the key intermediates **nxyT** were synthesized by palladium-catalysed Sonogashira reaction with different acetylenic alcohols and aryl bromides in one pot to gain a high yield of about 50% with purities higher than 99% (HPLC).

Using aryl iodine compounds as raw materials (Scheme 1), the target compounds were synthesized by sequential Heck coupling reaction, Sonogashira coupling reaction, deprotection of aldehyde and Wittig reaction. Classical organic synthetic reactions were employed in the above route to ensure the fast and efficient synthesis of target compounds; the synthesis processes and characterized data are shown in the supporting information. All target molecules and intermediate compounds were characterized and confirmed by ^{1}H NMR spectroscopy, ^{13}C NMR spectroscopy, mass spectroscopy and infrared spectroscopy.

3.2. Liquid crystal characterization

The phase transition temperatures and associated enthalpy changes of target compounds ***n*TFV**, **4TV**, **4FTV** and **4FTFV** were measured by differential scanning calorimetry (DSC). With reference to the reported mesophase textures and results from polarizing optical microscopy (POM), their liquid crystal phase textures were further confirmed and the corresponding data are summarized in Table S1 (ESI†). The POM pictures and DSC thermograms showed that all the target compounds display a stable nematic phase and a broad LC phase temperature range during the heating and cooling processes. In particular, the fluorine-substituted compound **4FTFV** possessed the broadest nematic temperature interval of 110.2 °C upon heating.

The representative DSC thermograms of compounds **2TFV** and **3TFV** are presented in Fig. 2(a and d). Compound **2TFV** exhibited a melting transition at 33.9 °C and a nematic to isotropic phase transition at 127.4 °C upon heating. The cooling process looks almost identical to the heating scan, except that a very large supercooled nematic mesophase range (119.1 °C) is observed, further indicating possible good low-temperature performance. Compound **2TFV** exhibited the typical schlieren texture of nematic mesophase upon heating and cooling (Fig. 2(b and c)). Similar to those of compound **2TFV**, the POM pictures and DSC thermogram of compound **3TFV** show an enantiotropic nematic mesophase with a broad temperature interval.

3.3. Thermal properties

The development of new LCs and an in-depth understanding of the correlation between molecular structure and thermal properties are essential for the further development of LC materials for LC photonics. Therefore, we investigated the effects of the lateral fluoro-substituent, central alkyne bond,

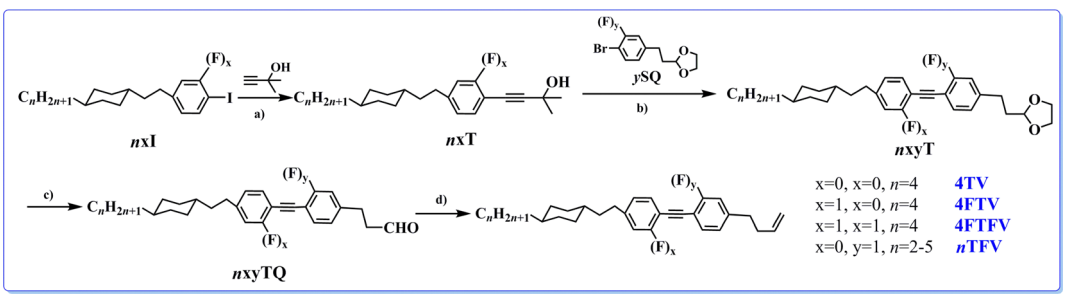

Scheme 1 Synthetic routes of compounds ***n*TFV**, **4TV**, **4FTV** and **4FTFV**. Reaction conditions: (a) Et_3N, CuI, $Pd(PPh_3)_4$, 80 °C, 8 h; (b) PhMe: H_2O (5 : 1, V/V), KOH, TBAB, $Pd(PPh_3)_4$, 80 °C, 8 h; (c) CHOOH, THF, 55 °C; (d) CH_3BrPPh_3, THF, −15 °C.

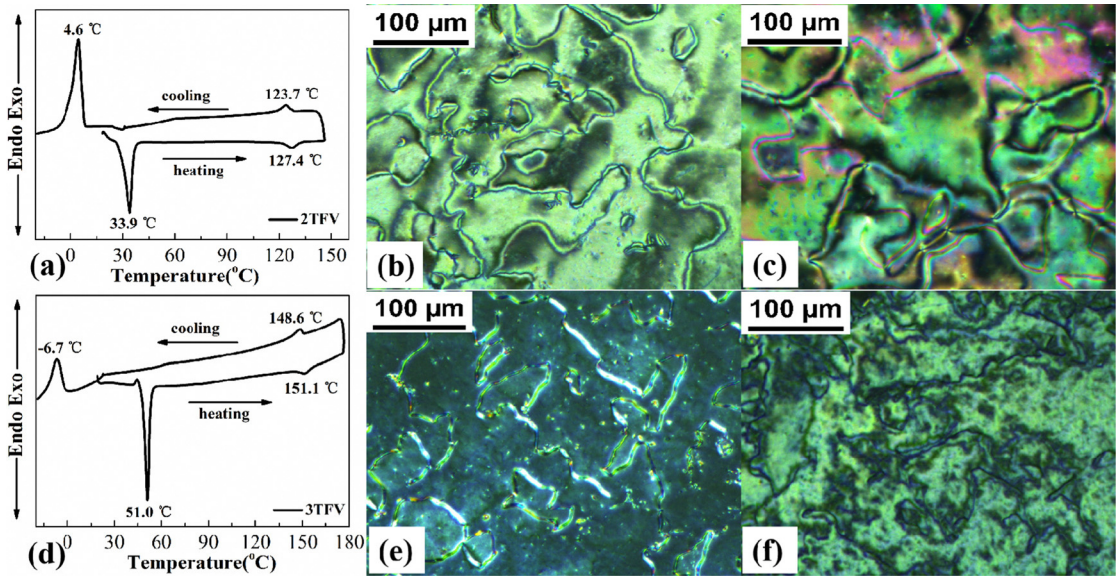

Fig. 2 DSC curves and POM images (×200) of compounds **2TFV** and **3TFV**. (a) DSC curve of **2TFV**; (b) schlieren texture of the nematic mesophase for **2TFV** at 56 °C on cooling; (c) schlieren texture of the nematic mesophase for **2TFV** at 120 °C on heating. (d) DSC curve of **3TFV**; (e) a nematic texture with surface disclination lines for **3TFV** at 127 °C on cooling; (f) a nematic thread-like texture for **3TFV** at 136 °C on heating.

terminal group and flexible *n*-alkyl chain on the thermal properties and the corresponding results are displayed in Fig. 3.

Overall, Fig. 3a shows that the melting points of the fluorinated LCs are lower than that of the non-fluorinated LC. The melting point of the non-fluorinated compound **4TV** is 100.2 °C

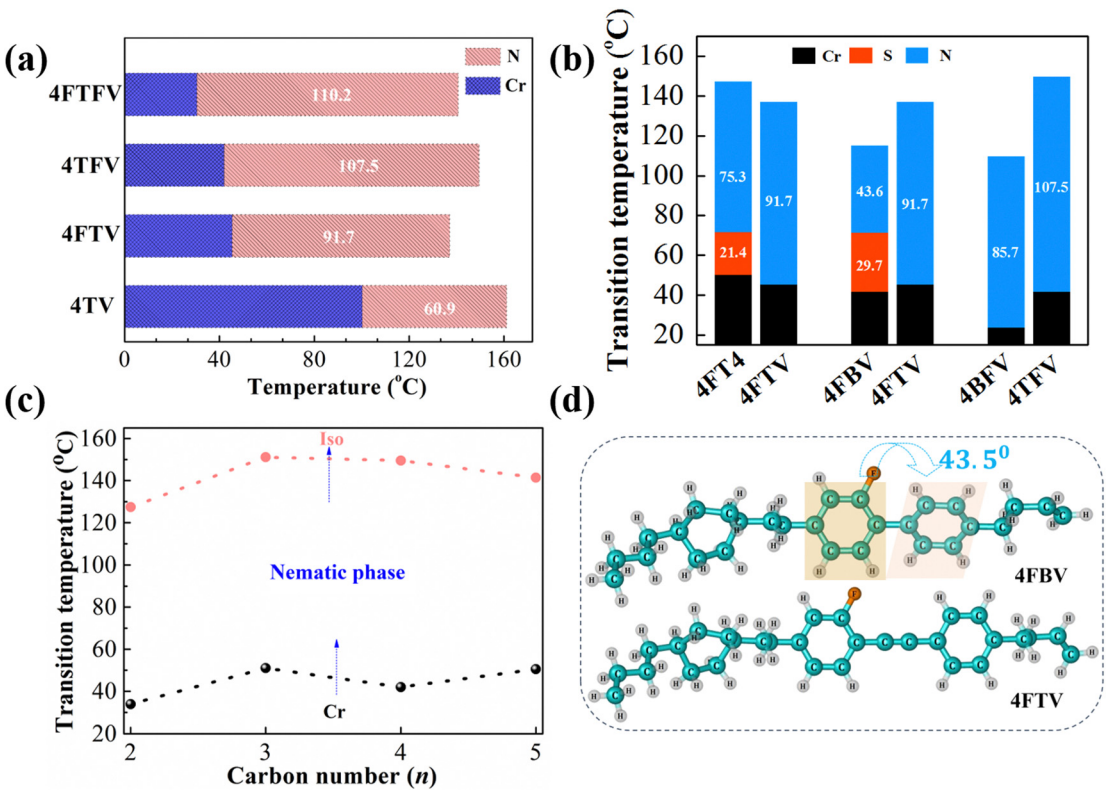

Fig. 3 (a) The mesophase ranges of compounds **4FTFV**, **4TFV**, **4FTV**, and **4TV** during heating; (b) effect of the acetylene bond and terminal alkenyl on phase transition temperature; (c) transition behaviour of the compounds ***n*TFV**: dependence of the transition temperatures on the carbon number (*n*) of the terminal alkyl chain. (d) Molecular structures of compounds **4FBV** and **4FTV** optimized at the DFT/b3lyp/6-311G (d,p) level of theory. Cr: crystal; N: nematic phase interval; S: smectic phase interval; Iso: isotropic liquid.

and the melting points of the mono-fluorinated compounds **4TFV** and **4FTV** are respectively 58.2 °C and 54.8 °C lower than that of **4TV**. Two *ortho* fluoro-substituents further decreased the melting point of **4TV** to the lowest value (30.5 °C), which is respectively 11.5 °C and 14.9 °C lower than those of mono-fluorinated **4TFV** and **4FTV**. It can be seen that the introduction of a lateral fluorine substituent is beneficial in decreasing the melting point of LC molecules, probably because lateral fluorine substituents reduce the degree of compact stacking between liquid crystal molecules. Meanwhile, the nematic phase temperature intervals of the fluorinated LC molecules **4FTFV**, **4TFV** and **4FTV** are respectively 49.3 °C, 46.6 °C and 30.8 °C wider than that of the non-fluorinated LC molecule **4TV**. It can be found that the introduction of a lateral fluorine substituent broadens the LC phase intervals. Furthermore, compound **4TFV** shows a lower melting point and a wider liquid crystal phase interval than compound **4FTV**, meaning that the lateral fluorine substituent group located on the second benzene ring facilitates a broader nematic phase interval.[43] This may be due to the lateral fluorine substituent located on the second benzene ring helping to increase the molecular aspect ratio (Table 1) and thus promoting the stability of the LC phase.[45]

The molecular structures of reference LC compounds **4FBV**, **4BFV**, **3BFV** and **4FT4** are shown in Fig. S5 (ESI†). From Fig. 3b, the melting and clearing points of compound **4FT4** with an *n*-butyl terminal group are 50.4 °C and 147.1 °C, respectively, with a liquid crystal phase interval of 96.7 °C and the presence of a smectic phase. Comparing **4FT4** with **4FTV**, it is found that replacing the *n*-butyl terminal group with a buty-3-enyl group could decrease the melting point and limit the smectic phase while maintaining a high clearing point and broad nematic phase interval. It has been speculated that the buty-3-enyl group increases the π–π interactions of the carbon–carbon double bond to inhibit the intertwining of the terminal alkyl chain, further facilitating the stability of the nematic phase.[43]

In Fig. 3d, it is seen that the biphenyl rings of **4FBV** are twisted to 43.5°, while the analogue **4FTV** containing a central alkyne bond is almost planar, which is conducive to molecular length and π–π interactions. As shown in Fig. 3b, the melting and clearing points of compound **4FBV** are 41.8 °C and 115.1 °C, respectively, with a liquid crystal phase interval of 73.3 °C and the presence of a smectic phase. Comparing **4FBV** with **4FTV**, it is seen that the insertion of the alkyne bond into the biphenyl rings broadened the mesomorphic phase temperature range, enhanced the melting and clearing points and suppressed the smectic phase.

Fig. 3c presents the effect of terminal alkyl chains (n = 2–5) on the melting and clearing points of compounds ***n*TFV** during the heating process. For the melting point, a clear even–odd effect is exhibited: compounds ***n*TFV** with even terminal chain lengths (n = 2, 4) exhibit lower melting points than those with odd terminal chain lengths (n = 3, 5). Meanwhile, compound **2TFV** has a lower clearing point than compound **3TFV**, but the longer the terminal alkyl chains (n = 4, 5) are, the lower the clearing points.

3.4. Physical properties

The fast response speed of liquid crystals is mainly associated with their properties of low viscosity and high Δn.[22,23] Therefore, we investigate the relationship between their molecular structures and their properties of birefringence and viscosity to lay the theoretical foundation for designing high Δn and low viscosity LC molecules. The new LC mixtures were prepared by separately adding compounds **4TV**, **4TFV**, **4FTV**, **4FTFV** and **3BFV** to the parent LC mixture **001** at a mass ratio of 15% and their Δn values all increased, as shown in Table 1. Compared to reference compound **3BFV**, the target molecules **4TV**, **4TFV**, **4FTV** and **4FTFV** exhibit larger Δn values of 0.28, 0.27, 0.26 and 0.24, respectively. It is obvious that the Δn value decreases from 0.28 to 0.24 with the increase of the lateral fluorine substitution number, which is attributable to the introduction of fluorine atoms into the benzene ring increasing the molecular width and weakening the intermolecular π–π conjugation.[44,49] Meanwhile, the numerical order of the viscosity value is consistent with that of birefringence, which indicates that large π-conjugation is beneficial to high birefringence, but not to low viscosity.

In addition, we evaluated the effects on the melting point and nematic phase temperature range of LC mixture **001** (Fig. 4). The parent LC mixture **001** has a melting point of 9.4 °C, a clearing point of 112.9 °C and a nematic phase temperature interval of 103.5 °C. Each of the five compounds **4TV**, **4FTV**, **4TFV**, **4FTFV** and **2TFV** (15 wt%) was dissolved in LC mixture **001**, yielding five new LC mixtures, termed **A**, **B**, **C**, **D** and **E**, respectively. It was found that, compared with parent LC mixture **001**, the melting points of the new mixtures were lower and their clearing points were increased, displaying wider nematic phase temperature intervals. Among these five compounds, compound **2TFV** decreased the original melting point of 9.4 °C to the lowest temperature (−1.6 °C) and maintained the widest nematic range (119.7 °C) of the LC mixtures.

3.5. Properties in high-Δn LC mixtures

The above results show that the target compounds display low melting point, wide nematic phase temperature interval, large birefringence and low rotational viscosity. They also effectively lower the melting point of LC mixture **001**, broaden its liquid crystal phase temperature interval, enhance its birefringence and maintain low rotational viscosity. To further evaluate their

Table 1 The DFT-calculated molecular length (L), width (W), and aspect ratios (L/W) of compounds **4TV**, **4TFV**, **4FTV** and **4FTFV** and their effects on the properties of LC mixture **001**

Compd.	L (Å)	W (Å)	L/W	T_m (°C)[a]	Nematic range (°C)[a]	Δn[a]	γ_1 (mPa s)[a]	Δn[b]
4TV	27.29	4.34	6.28	8.1	114.9	0.1095	391.9	0.2823
4TFV	27.25	5.32	5.12	1.4	117.8	0.1081	227.7	0.2730
4FTV	27.26	5.47	4.98	1.7	119.6	0.1067	159.3	0.2636
4FTFV	27.24	5.35	5.09	−0.2	116.5	0.1032	115.0	0.2418
3BFV	23.54	4.50	5.23	−7.6	113.9	0.0981	145.6	0.2063

[a] 85 wt% **001** + 15 wt% single compound. [b] Extrapolated experimental results.

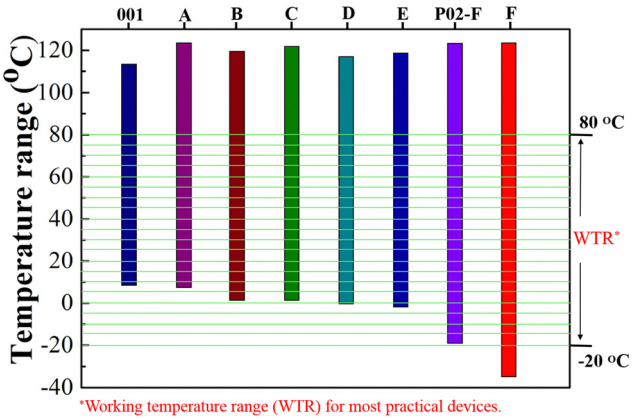

Fig. 4 Effect of target compounds on the temperature range of LC mixtures. Each of five compounds **4TV**, **4FTV**, **4TFV**, **4FTFV** and **2TFV** (15 wt%) was dissolved in LC mixture **001**, yielding new LC mixtures **A**, **B**, **C**, **D** and **E**. Compound **2TFV** (15 wt%) was dissolved in the LC mixture **P02-F**, yielding new LC mixture **F**.

properties in high-Δn LC mixtures, we selected the high-Δn LC mixture **P02-F** containing fluoro-tolane to investigate the effects on the properties of birefringence, rotational viscosity, low temperature and LC phase temperature interval (Table S2 and Fig. 4, ESI†).

Compound **2TFV** possesses the advantages of low melting point, wide nematic phase temperature interval and high birefringence and, therefore, it was selected as a typical representative of the target compounds to carry out the next study. Further experimental results showed that the addition of compound **2TFV** could lower the melting point of LC mixture **P02-F** to −34 °C, broaden its LC phase interval to 157.4 °C, and reduce its rotational viscosity to 185.5 mPa s while maintaining high birefringence (0.28). This predicts that the target compounds may have positive effects on the fast response time and wide operating temperature range of high-Δn LC mixtures. Thus, we prepared two LC mixtures **SNUP03** and **SNUP04** (Table S4 and S5, ESI†) according to the performance requirements of phase-only LCoS devices for AR displays[22,23] and further evaluated the comprehensive effect of compound **2TFV** on the performance of a high-Δn LC mixture; the test results are listed in Table 2.

As expected, adulteration with compound **2TFV** lowers the melting point of LC mixture **SNUP03** to −31.3 °C and broadens its LC phase temperature interval to 122.6 °C, meeting the operating temperature requirements for most indoor device applications. To further evaluate its effect on the response time of a phase-only liquid-crystal-on-silicon (LCoS) device for AR displays, we divided the phase change into nine levels (Table S3 and Fig. S5, ESI†) to evaluate the grayscale phase response. The phase-to-phase (PTP) response time was measured between every two phase levels and the experimental results are summarized in Table S4 (ESI†). In our experiment, the 2.08π phase change was achieved at an operation voltage of 5 V with a 3.12 μm transmissive LC cell. Since the response time is proportional to the square of the LC cell gap, the response time of the 1.56 μm reflective cell should be 4 times faster than that of the 3.12 μm transmissive cell. Therefore, the extrapolated average PTP response time of a 1.56 μm reflective LCoS panel is 2.89 ms, meaning that this phase-only LCoS could realize a 240 Hz refresh rate without overdrive circuitry. In recent years, the state-of-the-art LC material development for AR displays has reached a sub-millisecond response time for intensity modulation[23,25] and a ∼2 ms response time for 2π phase modulation[22,23,52] at 40 °C. To achieve broad temperature adaptability and fast response time, further research should focus on effective molecular tailoring strategies.

Table 2 Measured properties of the two LC mixtures at T = 40 °C, λ = 633 nm, and f = 1 kHz

No.	T_m (°C)	T_c (°C)	Δn	$\Delta\varepsilon$	γ_1 (mPa s)	K_{11} (pN)	V_{th} (V)
SNUP03	−7.5	89.9	0.27	7.25	75.1	8.5	1.04
SNUP04	−31.3	91.3	0.26	6.31	97.4	7.9	1.18

4. Conclusion

The molecular tailoring strategy was applied to obtain novel fluorinated tolane-liquid crystals comprised of a tolane central core, *trans* cyclohexyl core, ethylene bridge, buty-3-enyl terminal group, lateral fluorine atom and terminal alkyl chain. These target compounds exhibited enantiotropic nematic mesophases with a broadest nematic temperature interval of 110.2 °C and lowest melting point of 30.5 °C and the melting points of compounds ***n*TFV** exhibited a clear even–odd effect. The correlation between molecular structure and thermal properties indicated that the lateral fluoro-substituent and the buty-3-enyl terminal group helped to broaden the nematic phase interval, decrease the melting point and suppress the smectic phase, which corroborates the DFT calculations. Meanwhile, the fluorinated tolane liquid crystals with the buty-3-enyl terminal group displayed high Δn values (0.24–0.27) and can effectively lower the melting point, broaden the LC phase temperature interval, and maintain the high Δn and low γ_1 of three LC mixtures (**001**, **P02-F** and **SNUP03**). Finally, we developed a new LC mixture (**SNUP04**) by mixing compound **2TFV** and other compounds for phase-only LCoS-based AR displays, which could enable a 240 Hz frame rate at an operation voltage of 5 V and 2.08π phase change. This molecular tailoring strategy can be an effective way to accomplish the integration of many desired properties into one compound and the compound developed herein is confirmed to be an effective LC dopant to improve the ambient temperature tolerance of LC mixtures.

Conflicts of interest

There are no conflicts to declare.

Acknowledgements

The authors thank for the financial support by the National Natural Science Foundation of China (62105194, 52273186 and 51873100), the China Postdoctoral Science Foundation

(2022T150394), Sanqin scholars innovation teams in Shaanxi Province, China, International Science and Technology Cooperation Project of Shaanxi Province, China (2021KW-20) for financial support of this work. We are grateful to Professor Wenliang Wang at Shaanxi Normal University for theoretical calculations.

References

1 K. S. Lee, S. Maurya and Y. S. Kim, *et al.*, Intermediate temperature fuel cells via an ion-pair coordinated polymer electrolyte, *Energy Environ. Sci.*, 2018, **11**, 979–987.
2 X. Zhang, X. Fu and S. Yang, *et al.*, Design of sepiolite-supported ionogel-embedded composite membranes without proton carrier wastage for wide-temperature-range operation of proton exchange membrane fuel cells, *J. Mater. Chem. A*, 2019, **7**(25), 15288–15301.
3 Y. Chen, S. Tan and N. Li, *et al.*, Self-elimination of intrinsic defects improves the low-temperature performance of perovskite photovoltaics, *Joule*, 2020, **4**(9), 1961–1976.
4 G. Li, Z. Su and M. Li, *et al.*, Structure and Performance Evolution of Perovskite Solar Cells under Extreme Temperatures, *Adv. Energy Mater.*, 2022, **12**(48), 2202887.
5 C. S. Rustomji, Y. Yang and T. K. Kim, *et al.*, Liquefied gas electrolytes for electrochemical energy storage devices, *Science*, 2017, **356**, eaal4263.
6 L. Cheng, Y. Wang and J. Yang, *et al.*, An Ultrafast and Stable Li-Metal Battery Cycled at – 40 °C, *Adv. Funct. Mater.*, 2022, 2212349.
7 T. Ma, Y. Ni and Q. Wang, *et al.*, Optimize Lithium Deposition at Low Temperature by Weakly Solvating Power Solvent, *Angew. Chem., Int. Ed.*, 2022, **134**, e202207927.
8 Q. Liu, A. Zhao and X. He, *et al.*, Full Temperature All Solid State Ti3C2Tx/Aramid Fiber Supercapacitor with Optimal Balance of Capacitive Performance and Flexibility, *Adv. Funct. Mater.*, 2021, **31**, 2010944.
9 X. Hou, Q. Zhang and L. Wang, *et al.*, Low-temperature-resistant flexible solid supercapacitors based on organohydrogel electrolytes and microvoid-incorporated reduced graphene oxide electrodes, *ACS Appl. Mater. Interfaces*, 2021, **13**, 12432–12441.
10 G. E. Bauman, J. M. McCracken and T. J. White, Actuation of Liquid Crystalline Elastomers at or Below Ambient Temperature, *Angew. Chem., Int. Ed.*, 2022, e202202577.
11 Y. Chen, C. Zheng and W. Yang, *et al.*, Over 200 °C Broad Temperature Lasers Reconstructed from a Blue Phase Polymer Scaffold, *Adv. Mater.*, 2022, 2206580.
12 W. Hu, L. Wang and M. Wang, *et al.*, Ultrastable liquid crystalline blue phase from molecular synergistic self-assembly, *Nat. Commun.*, 2021, **12**, 1440.
13 N. Gao, S. Jing and X. Kong, *et al.*, Low-temperature properties of nematic liquid crystal materials for display, *Liq. Cryst.*, 2021, **48**(11), 1593–1607.
14 J. Xiong, E. L. Hsiang and Z. He, *et al.*, Augmented reality and virtual reality displays: emerging technologies and future perspectives, *Light: Sci. Appl.*, 2021, **10**, 216.
15 Y. Li, Q. Yang and J. Xiong, *et al.*, 3D displays in augmented and virtual realities with holographic optical elements, *Opt. Express*, 2021, **29**, 42696–42712.
16 K. Yin, E. L. Hsiang and J. Zou, *et al.*, Advanced liquid crystal devices for augmented reality and virtual reality displays: principles and applications, *Light: Sci. Appl.*, 2022, **11**, 1–22.
17 Y. Li, S. Chen and H. Liang, *et al.*, Ultracompact multifunctional metalens visor for augmented reality displays, *PhotoniX*, 2022, **3**, 29.
18 M. Mrukiewicz, K. Kowiorski and P. Perkowski, *et al.*, Threshold voltage decrease in a thermotropic nematic liquid crystal doped with graphene oxide flakes, *J. Biomed. Nanotechnol.*, 2019, **10**, 71–78.
19 M. Yousefi, S. M. Rozati and N. Najafi, *et al.*, Investigation of the effect of temperature on the structural, optical, electrical, and self-cleaning properties of ITO thin films, *Appl. Phys. A: Mater. Sci. Process.*, 2020, **126**(4), 455–459.
20 S. Yang, S. Wang and H. Liao, *et al.*, Improving the performance of Cu2ZnSnS4 thin film solar cell by engineering the ITO film thickness, *Physica B*, 2020, **589**(10), 412196.
21 L. Yu and Y. S. Qian Technology, of rugged AM-LCD under lower temperature, *Chin. J. Liq. Cryst. Disp.*, 2003, **18**(5), 342–347.
22 R. Chen, Y. Huang and J. Li, *et al.*, High-frame-rate liquid crystal phase modulator for augmented reality displays, *Liq. Cryst.*, 2019, **46**(2), 309–315.
23 Y. Huang, Z. He and S. T. Wu, Fast-response liquid crystal phase modulators for augmented reality displays, *Opt. Express*, 2017, **25**(26), 32757–32766.
24 Q. Yang, J. Zou and Y. Li, *et al.*, Fast-response liquid crystal phase modulators with an excellent photostability, *Crystals*, 2020, **10**(9), 765.
25 H. Chen, F. Gou and S. T. Wu, Submillisecond-response nematic liquid crystals for augmented reality displays, *Opt. Mater. Express*, 2017, **7**(1), 195–201.
26 R. Chen, L. Wang and Z. An, *et al.*, Effect of π-conjugation units on the liquid crystal and photovoltaic performance of heterocyclic pyridine-based compounds, *Liq. Cryst.*, 2021, **48**(15), 2178–2187.
27 R. Chen, Y. Qin and Z. An, *et al.*, The effect of phenyl ring on the physical properties of liquid crystals containing 4-pyridyl terminal group, *Liq. Cryst.*, 2018, **45**, 1825–1833.
28 N. Xie, S. Du and R. Chen, *et al.*, Synthesis and properties of benzoxazole-terminated mesogenic compounds containing tolane with high birefringence and large dielectric anisotropy, *Liq. Cryst.*, 2021, **48**, 1978–1991.
29 R. Dąbrowski, J. Dziaduszek and A. Ziółek, *et al.*, Low viscosity, high birefringence liquid crystalline compounds and mixtures, *Opto-Electron. Rev.*, 2007, **15**(1), 47–51.
30 H. Chen, Y. Liu and M. Chen, *et al.*, Research of Liquid-Crystal Materials for a High-Performance FFS-TFT Display, *Molecules*, 2023, **28**, 754.
31 M. Bremer, M. Klasen Memmer and D. Pauluth, *et al.*, Novel liquid crystal materials with negative dielectric anisotropy for TV application, *J. Soc. Inf. Disp.*, 2006, **14**, 517–521.

32 M. Hu, J. Li and Z. Yang, *et al.*, Synthesis and properties of difluoromethyleneoxy-bridged liquid crystals terminated by 2,2-difluorovinyloxy group, *Liq. Cryst.*, 2015, **42**, 383–389.
33 Y. Arakawa, S. Kang and H. Tsuji, *et al.*, The design of liquid crystalline bistolane-based materials with extremely high birefringence, *RSC Adv.*, 2016, **6**, 92845–92851.
34 N. Li, Z. Li and X. Zhang, *et al.*, Synthesis of 1, 4-bis (phenylethynyl) benzenes and their application as blue phase liquid crystal composition, *Int. J. Mol. Sci.*, 2013, **14**, 23257–23273.
35 J. Li, X. Yang and N. Gan, *et al.*, The effect of lateral fluorination on the properties of phenyl-tolane liquid crystals, *Liq. Cryst.*, 2015, **42**, 397–403.
36 Q. Weng, L. Zhao and R. Chen, *et al.*, Syntheses of new diluents for medium birefringence liquid crystals materials, *Liq. Cryst.*, 2019, **46**, 700–707.
37 J. Li, M. Hu and R. Chen, *et al.*, Low dielectric loss and good miscibility of the tolane liquid crystals by tuning their lateral substituents, *J. Mol. Liq.*, 2021, **325**, 115236.
38 R. Dąbrowski, P. Kula and J. Herman, High birefringence liquid crystals, *Crystals*, 2013, **3**, 443–482.
39 R. Chen, L. Zhao and Z. An, *et al.*, Synthesis and properties of allyloxy-based tolane liquid crystals with high negative dielectric anisotropy, *Liq. Cryst.*, 2017, **44**, 2184–2191.
40 P. Kirsch and M. Bremer, Nematic liquid crystals for active matrix displays: molecular design and synthesis, *Angew. Chem., Int. Ed.*, 2000, **39**, 4216–4235.
41 M. Schadt, Linear and non-linear liquid crystal materials, electro-optical effects and surface interactions. Their application in present and future devices, *Liq. Cryst.*, 1993, **14**(1), 73–104.
42 Y. Goto, K. Kitano and T. Ogawa, Liquid crystals of some new tolane derivatives containing a 1, 2-ethylene linkage, *Liq. Cryst.*, 1989, **5**(1), 225–232.
43 Y. Jiang, Z. An and P. Chen, *et al.*, Synthesis and mesomorphic properties of but-3-enyl-based fluorinated biphenyl liquid crystals, *Liq. Cryst.*, 2012, **39**(4), 457–465.
44 R. Chen, Z. An and W. Wang, *et al.*, Improving UV stability of tolane-liquid crystals in photonic applications by the ortho fluorine substitution, *Opt. Mater. Express*, 2016, **6**(1), 97–105.
45 R. Chen, Z. An and F. Li, *et al.*, Synthesis and physical properties of tolane liquid crystals containing 2, 3-difluorophenylene and terminated by a tetrahydropyran moiety, *Liq. Cryst.*, 2016, **43**(4), 564–572.
46 S. Zhu, R. Chen and W. Zhang, *et al.*, Dissecting terminal fluorinated regulator of liquid crystals for fine-tuning intermolecular interaction and molecular configuration, *J. Mol. Liq.*, 2020, **310**, 113225.
47 M. Hu, Z. An and J. Li, *et al.*, Low mid-infrared absorption tolane liquid crystals terminated by 2, 2-difluorovinyloxyl: synthesis, characterization and properties, *J. Mater. Chem. C*, 2016, **4**, 4939–4945.
48 R. Chen, Z. An and W. Wang, *et al.*, Lateral substituent effects on UV stability of high-birefringence liquid crystals with the diaryl-diacetylene core: DFT/TD-DFT study, *Liq. Cryst.*, 2017, **44**(10), 1515–1524.
49 R. Chen, Y. Jiang and J. Li, *et al.*, Dielectric and optical anisotropy enhanced by 1, 3-dioxolane terminal substitution on tolane-liquid crystals, *J. Mater. Chem. C*, 2015, **3**, 8706–8711.
50 Z. Luo, F. Peng and H. Chen, *et al.*, Fast-response liquid crystals for high image quality wearable displays, *Opt. Mater. Express*, 2015, **5**(3), 603–610.
51 R. Chen, Z. An and X. Chen, *et al.*, Syntheses and properties of four-ring liquid crystals with ethylene and internal alkyne bridge, *Chem. J. Chin. Univ.*, 2014, **35**, 1433–1438.
52 Y. Huang, E. Liao and R. Chen, *et al.*, Liquid-crystal-on-silicon for augmented reality displays, *Appl. Sci.*, 2018, **8**(12), 2366.